IN VIVO COMPARTMENTAL RELAXATION IN A MODEL OF GRADED MUSCLE EDEMA

By

Jack T. Skinner

Thesis

Submitted to the Faculty of the

Graduate School of Vanderbilt University

in partial fulfillment of the requirements

for the degree of

MASTER OF SCIENCE

in

Biomedical Engineering

May, 2009

Nashville, Tennessee

Approved:

Mark D. Does

Bruce M. Damon

ACKNOWLEDGEMENTS

I would like to thank my advisor, Dr. Mark Does, for all his help and guidance during this research and thesis preparation. I would also like to thank Dr. Bruce Damon for his input during the completion of this thesis. Also, many thanks go to Jarrod True for animal support and help with experimental setup. Finally, I would like to thank my wife, Stephanie, for her patience and support throughout this process.

TABLE OF CONTENTS

LIST OF TABLES

LIST OF FIGURES

CHAPTER I

INTRODUCTION

I.1 Evaluation of Skeletal Muscle Injury with MRI

Muscle injury is a common condition that may result from pathology or trauma such as contusions or strains. Magnetic Resonance Imaging (MRI) provides an excellent way of visualizing this type of muscle damage by means of image contrast between normal and injured muscle tissue. Variations in image signal intensity indicate changes in Nuclear Magnetic Resonance (NMR) signal characteristics, specifically tissue relaxation times, T_1 and T_2. Pathological conditions affecting skeletal muscle may result in an alteration in muscle size, shape, or signal intensity [1]. Muscular diseases such as polymyositis and dermatomyositis have been shown to cause a change in MRI signal intensity due to the presence of muscle edema [2]. As a result of the increase in intracellular or extracellular free water associated with the edema, T_2 weighted images of muscle injury will present with increased signal. The amount of muscle edema on an MRI image has been shown to correlate with the severity of the disease as well as helping in locating the injury itself when making a differential diagnosis [3,4].

Though the appearance of muscle edema on a T_2 weighted image is helpful in diagnosis, its utility in a clinical setting is mostly qualitative. These MR images may prove useful in guiding tissue biopsies of diseased muscle or in locating strains and tears, but there exists a lack of knowledge in the clinic to take full advantage of the sub-voxel information that can be probed from the tissue. It would be desirable to obtain a quantitative relationship between the muscle injury and the extracted MRI parameters (i.e. relaxation times, diffusion coefficients, etc.). Specifically, determining the relationship between varying amounts of edema and changes in relaxation times is of importance. This relationship might offer a less invasive manner of diagnosing muscle pathologies and injuries through a more complete understanding of compartmental relaxation and water exchange in edematous muscle.

I.2 Muscle Edema

Edema can be described as an excess accumulation of interstitial fluid in a tissue. An abnormal increase in signal intensity in a T_2 weighted image of skeletal muscle may be indicative of "muscle edema". Muscle edema may be focal with ill-defined and poorly circumscribed margins or may only diffusely involve a muscle [1]. As previously stated, this edema can arise from direct insult, pathologies, or even from exercise [5]. The generation of edema in tissue is controlled by the Starling equation and is a result of an imbalance between hydrostatic and oncotic forces. The hydrostatic and oncotic pressures oppose one another and aid in the movement of fluid across the capillary membranes. The oncotic pressure is a form of osmotic pressure exerted by the proteins in the blood plasma. Edema can occur in tissue as a result of inflammation, increased hydrostatic pressure, or reduced oncotic pressure as is true with states of low plasma osmolality.

I.3 Relaxation Measurements in Skeletal Muscle

I.3.1 *Transverse Relaxation (T_2)*

Changes in the T_2 of muscle tissue can offer some insight into micro-anatomical alterations associated with muscle injury and inflammation. Methods for measuring transverse relaxation are described below. Following an RF excitation pulse, spins that are oriented in the transverse plane will experience both an applied field and fluctuations in a local magnetic field due to interactions with neighboring spins. Variations in the local magnetic field (B) as well as interactions among spins lead to different local precessional frequencies according to the Larmor equation

$$\omega = \gamma B \qquad \text{(Eq. 1)}$$

where ω is the frequency of precession, γ is the gyromagnetic ratio (26,747 rads/(s·G) for H^1), and B is the local magnetic field [6]. The spins precess at various frequencies which results in transverse signal decay owing to a loss of phase coherence. At this point the spins are said to be 'dephasing'. The dephasing of spins leads to a reduction in the net transverse magnetization vector. This entire process is known as spin-spin relaxation and the rate at which the transverse magnetization decays is known as R_2. The associated time constant is $1/R_2$ or T_2.

In order to quantitatively measure T_2, multiple spin-echo experiments are performed. To form a spin echo, longitudinal magnetization is first rotated down into the transverse plane by a 90° RF pulse. The magnetization that has been placed in the transverse plane begins to acquire phase during a period, τ. A 180° refocusing pulse is then applied, which reverses the phase acquired during τ. If the field gradients experienced by the spins are static, then the phase acquired before the 180° pulse will be refocused during a second time period, τ, and a spin echo will form (at $t=2\tau$). In a multiple spin-echo (ME) sequence the 90° pulse is followed by several 180° refocusing pulses which are used to form a train of echoes that are separated by a time TE. The signal intensity at each echo is used to form a decay curve that can be fitted to extract the T_2 value of the tissue.

In a homogenous environment, the transverse magnetization after excitation can be described by a monoexponential decay

$$M_{\perp}(t) = M_{\perp}(0)e^{-t/T_2} \tag{Eq. 2}$$

where $M_{\perp}(0)$ is the transverse magnetization immediately following the excitation pulse and t is the time for spin echo formation relative to the excitation. In tissue there are additional constituents such as proteins and membrane bound molecules that can interact with water molecules and have an effect on the local magnetic field, and therefore, the observed T_2. The rate at which transverse magnetization decays in tissue is related to the interaction of water molecules with the surrounding environment. Mechanisms that prevent the water molecules from interacting with each other can alter their behavior such that the observed signal can not be explained by a monoexponential decay. The presence of transverse magnetization whose decay can be described by multiple T_2 values is known as multiexponential T_2 (MET_2) decay.

As early as 1969, there was evidence that two phases of water existed in skeletal muscle and the phenomena that explained these two distinct signals involved the restriction of the motional freedom of the water molecules [7]. In 1974, Hazlewood *et al.* suggested that not only was there a minimum of two phases of ordered water in skeletal muscle, but there appeared to be three different fractions of exchanging water in rat skeletal muscle, corresponding to three distinct T_2 times [8]. The three components were designated as hydration water molecules of protein and macromolecules (7% of muscle water, T_2<1ms), myoplasm or intracellular water (83% of muscle water, T_2~44ms), and extracellular space (10% of muscle water, T_2~155ms). The multi-exponential signals obtained from muscle tissue continued to be of interest, though the origin of the non-monoexponentiality was disputed [9,10].

In 1993 Cole presented a study in which support for the physical compartmentation model was strengthened when it was found that maceration of skeletal muscle resulted in a loss of biexponential T_2 decay, specifically a loss of the long T_2 component [11]. This result lends itself to the idea that the observed biexponential signal can be attributed to intracellular and extracellular compartments. In recent years, several other studies observed biexponential T_2 decay by inducing edema in skeletal muscle. The biexponential decay was attributed to swelling in the intra- and extracellular compartments [12,13,14].

I.3.2 *Longitudinal Relaxation (T_1)*

In addition to changes in T_2, the spin-lattice relaxation time (T_1) can also provide information about tissue pathology or injury. Following an RF excitation, the transverse component of the magnetization decays as the longitudinal component returns towards equilibrium along the direction of the B_o field. The longitudinal component of the magnetization, M_z, following an RF pulse applied at equilibrium, can be described by

$$M_z(t) = M_o - M_o(1-\cos(\theta))e^{-t/T_1} \quad \text{(Eq.3)}$$

where M_o represents the magnetization at thermal equilibrium and θ is the flip angle of the RF pulse. Longitudinal relaxation involves the exchange of energy between the hydrogen nuclei and the surrounding lattice. Randomly fluctuating magnetic fields caused by motion of surrounding magnetic dipoles enhances energy exchange and therefore enhances, or shortens T_1 [15]. Accordingly, the T_1 in tissue will be dependent on field strength. Based on the size of the molecules in tissue and their tumbling frequencies, as the field strength is increased and the Larmor frequency increases, the energy at the Larmor frequency will eventually begin to decrease and the relaxation time T_1 will become longer.

There exists several ways to measure T_1, based on the flip angle dependent magnetization in Eq. 3. One of these methods is a saturation recovery measurement. In a saturation recovery (SR) experiment, a 90° RF pulse is applied followed by the acquisition of either a gradient echo or spin echo. The echo is followed by a period of time in which the spins in the transverse plane are allowed to dephase while the longitudinal component of the magnetization returns toward equilibrium. This experiment is repeated for various repetition times both shorter and longer than the expected T_1 of the tissue to characterize the T_1 regrowth curve.

As with transverse relaxation measurements in edematous muscle *in vivo*, longitudinal relaxation measurements can also be made to characterize the micro-anatomical structure of the tissue. Longitudinal relaxation has been measured in normal skeletal muscle as early as 1974 [16]. In a study to compare normal and tumorous rat tissues, Block and Maxwell found the T_1 in ex vivo rat muscle at 2.35 T to be 1.138s. In another study in which an integrated T_1-T_2 measurement was made, English *et al*. showed that for both fast and slow twitch rat muscle *ex vivo* at 0.59 T the corresponding T_1 was about 640 ms [17]. In 1993 de Certaines *et al*. published a multi-center MRI study on in vivo measurements of proton relaxation times in humans [18]. This study found the T_1 of normal human skeletal muscle to be 1.183s at 1.5 T and the T_2 to be 33ms at 1.5 T.

A more recent study by Saab *et al*. also utilized a two-dimensional relaxometry sequence to characterize skeletal muscle *in vivo* at 3T [19]. In this study an IR-CPMG pulse sequence was modified in order to make *in vivo* measurements at high SNR. Saab found that human skeletal muscle *in vivo* exhibits not one but four distinct compartments with corresponding T_1 and T_2 relaxation times. The T_1 for the two largest compartments making up ~89% of the signal was found to be ~1.4s. At 7T, Faure *et al*. found the T_1 of skeletal muscle in rat paw to be 1.44 ± 0.07s [20]. The same study also found the T_2 of normal skeletal muscle at 7T to be 20.2 ± 1.0ms. Few groups have reported T_1 measurements of *in vivo* skeletal muscle at higher fields (7T and above). At the time of this study, the T_1 of muscle at 9.4T was unknown to the author. In addition, reports of *in vivo* multiexponential T_1 (MET_1) in skeletal muscle with injury were not available. Though it is known that T_2 is multiexponential in nerve, injured muscle, etc., the observation of multiexponential T_1 is less common. MET_1 can be more readily observed by combining T_1 and T_2 measurements; this is known as two-dimensional relaxometry. The utility of two-dimensional relaxometry in this thesis is important in attempting to probe sub-voxel information from tissue compartments of edematous muscle.

I.3.3 *Integrated Relaxometry Measurements*

Interpreting T_1 and T_2 measurements of compartmental muscle water *in vivo* can be very challenging. The presence or absence of multiexponential relaxation can be difficult to interpret, and may be dependent on the severity of edema. The heterogeneity of the tissue itself also makes the process of making accurate measurements of water fractions based on relaxation times a challenge. The implementation of two-dimensional relaxometry measurements helps reveal correlations between T_1 and T_2 relaxation components as they relate to individual spin groups [17].

These particular measurements have been made by several groups. As previously mentioned, English *et al*. used an integrated pulse sequence, inversion recovery prepared Carr-Purcell-Meiboom-Gill (IR-CPMG), to measure both T_1 and T_2 in *ex vivo* rat muscle [17]. In another study, Snaar and Van As made simultaneous measurements of T_1 and T_2 by combining saturation recovery and CPMG pulse sequences (SR-CPMG) [21]. It was shown that integrated T_1-T_2 measurements in a non-exchanging system resulted in distinct T_1 values for each T_2 value due to an improvement in SNR and amplitude information of the water fractions from the incorporated T_2 measurements. Observations of MET_1 were more apparent in integrated T_1-T_2 measurements when compared to simple IR or SR measurements. A similar method was implemented by Does and Gore in order to observe MET_1 in rat trigeminal nerve *in vivo* [22]. Does used a saturation recovery prepared multiple spin-echo (SR-ME) imaging sequence with rapid acquisition to help reveal three distinct T_1-T_2 components. As previously mentioned, Saab *et al*. used a single voxel IR-CPMG sequence to make T_1-T_2 measurements of skeletal muscle *in vivo*.

I.4 Edema Injury Model

Several models exist that explore non-disease induced edema in skeletal muscle. The most common of these models, due to its utility in human imaging, is an exercise induced edema model [23-25]. As metabolic expense and perfusion increase with exercise, net water transfer occurs between vascular and extravascular compartments and total muscle water content increases [24]. This increase in muscle water can then be imaged. The majority of these studies observe the changes in transverse relaxation (T_2) and diffusion in skeletal muscle with exercise. In small animals, electroporation injury is used to model edematous muscle and look at changes in muscle tissue after membrane trauma [26,27]. Yet another model focuses on compression-induced deep tissue injury and how damage to the muscle fibers results in edema and inflammation, as well as necrosis with a complete disorganization of the internal muscle fiber structure [28]. As a result of injury T_2-weighted images show localized areas of increased signal intensity. Early studies cite an increase in extracellular fluid volume as the explanation for an increase in T_2 [24,25]. Other studies argue that increases in T_2 are not primarily associated with increases in extracellular and vascular fluids but are dominated by relaxation in the much larger intracellular fluid compartment [23].

Aside from physically inducing edema through exercise, pressure, insult, etc., edema can be induced through an injected substance. A study by Gambarota *et al*.

showed how injections of saline of various tonicities into rat skeletal muscle produced multiexponential transverse relaxation [12]. As a result of the injections, both fast and slow decaying T_2 components were observed in the muscle. The osmotic manipulation of the compartment sizes extracted from edematous muscle allowed the assignment of the fast and slow T_2 components to intracellular and extracellular water, respectively.

The injection of a chemical agent, such as λ-carrageenan, is another common mode of inducing edema in muscle. Known for its use in the development of non-steroidal anti-inflammatory drugs, the carrageenan-induced edema model is often seen in the rat paw as a way to simulate an inflammatory response [29,30]. Carrageenan-induced edema is mediated in a temporal manner by serotonin and histamine at first, then kinins, and finally prostaglandins about 3 hours after injection [31,32]. In a study by Ababneh *et al*. the carragenan-induced paw edema (CIPE) model was implemented with MRI to measure changes in diffusion parameters and transverse relaxation [13]. The study found that although the two T_2 components could be assigned to intra- and extracellular compartmentalization, the measure of bi-exponential diffusion could not be associated in the same way with confidence. A more recent study by Fan and Does focused on λ-carrageenan induced edema in the rat hindlimb and its effects on transverse relaxation resolved diffusion measurements [14]. The results of this study showed that the elevated apparent diffusion coefficient (ADC) and decreased fractional anisotropy (FA) in the long-lived muscle water component reflects a relatively unrestricted and less ordered space due to a combination of swelling and muscle fiber necrosis. It was postulated that the short-lived edematous muscle signal could be ascribed to water from uninjured muscle fibers, therefore reflecting intracellular water contribution to normal muscle signal [14]. The interpretation of these previously described measurements is made difficult in part by the effect of water exchange between tissue compartments.

I.5 Inter-compartmental Exchange

In this study, we model muscle tissue with two well-mixed exchanging compartments. Each compartment has its own pool size, or equilibrium magnetization, M_0, as well as its own relaxation times, T_1 and T_2, and mean water residence time, τ. A representation of this model can be seen in Fig. I.1. From this model, and subsequent mathematical manipulation, we can determine how relaxation rates are affected by inter-compartmental exchange.

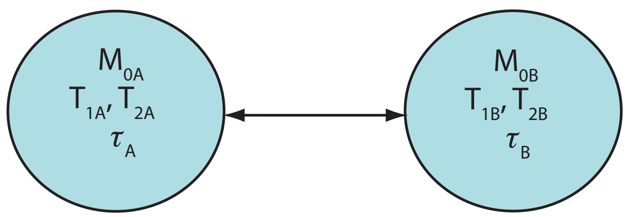

Figure. I.1. Two-compartment model. Each compartment has its own relaxation rates, R_1 and R_2, equilibrium magnetization, and mean water residence times, τ_A and τ_B.

The Bloch-McConnell equations describe the effect of exchange on the aforementioned two-compartment model [33]. The Bloch-McConnell equations for the case of longitudinal magnetization are seen in Eq. 4a and Eq. 4b:

$$\frac{dM_{ZA}(t)}{dt} = \frac{1}{T_{1A}}\left[M_{0A} - M_{ZA}(t)\right] - \frac{M_{ZA}}{\tau_A} + \frac{M_{ZB}}{\tau_B} \qquad \text{(Eq. 4a)}$$

$$\frac{dM_{ZB}(t)}{dt} = \frac{1}{T_{1B}}\left[M_{0B} - M_{ZB}(t)\right] - \frac{M_{ZB}}{\tau_B} + \frac{M_{ZA}}{\tau_A} \qquad \text{(Eq. 4b)}$$

The $-M_{ZA}/\tau_A$ term in Eq. 4a measures the rate at which M_{ZA} decreases due to transfer out of compartment A and $+M_{ZB}/\tau_B$ measures the rate at which M_{ZA} increases due to transfer into compartment A. The logic is similar for Eq. 4b. Equations similar to 4a and 4b can be formulated for the case of transverse magnetization. The solution to Eq. 4 represents the observable or apparent relaxation rates, $\frac{1}{\hat{T}_{iS,L}}$, for each compartment [34]. This solution is seen in Eq. 5.

$$\frac{1}{\hat{T}_{1S,L}} = \tfrac{1}{2}\left[\frac{1}{T_{1A}} + \frac{1}{\tau_A} + \frac{1}{T_{1B}} + \frac{1}{\tau_B}\right] \pm \tfrac{1}{2}\sqrt{\left[\left(\frac{1}{T_{1A}} + \frac{1}{\tau_A} - \frac{1}{T_{1B}} - \frac{1}{\tau_B}\right)^2 + \frac{4}{\tau_A \tau_B}\right]} \qquad \text{(Eq. 5)}$$

The process of accurately measuring relaxation times and proton densities in the presence of exchange can be difficult. When exchange is present, the relaxation times and spin density fractions that are measured represent apparent or observable quantities, not necessarily the *actual* relaxation times and spin densities. The relative magnitude of the exchange rate, whether fast or slow, will dictate the accuracy of the observed parameters.

It is possible that compartments in a biological system can be in one exchange regime on a T_1 timescale but in another exchange regime on a T_2 timescale [35]. If a system is in fast exchange, then an averaged relaxation rate may be produced, yielding monoexponential relaxation that masks information about the individual spin populations. If, however, the system is in slow or intermediate exchange, relaxation rates are distinct, and multiexponential relaxation can be observed. If the system is in slow exchange then the inverse of the average intracellular and extracellular lifetimes, τ_a and τ_b, together, is much less than the difference in relaxation rates, R_a and R_b, of the two spin groups, or

$$\left[\frac{1}{\tau_A}+\frac{1}{\tau_B}\right] << \left[\left|R_b - R_a\right|\right] \qquad \text{(Eq. 6)}$$

In the same way if the left side of Eq. 6 is much greater than the right side the system is said to be in fast exchange and if they are approximately equal, they are said to be in intermediate exchange [34]. In the slow exchange regime, the measured volumes of each spin group or compartment approaches the actual volume corresponding to their proton concentrations.

I.6 Two Pool Models of Muscle

In the two pool model of muscle, as has been previously described, we define each pool as having its own T_1 and T_2 values that describe the relaxation process in that pool. Conceptually, this model describes two components that could be extracted from a T_1-T_2 spectrum. However, if the two pools are in exchange with one another, this is not necessarily the case. If the two pool system is in neither extreme exchange regime, on a T_1 time scale, solving the Bloch-McConnell equations for M_Z (as in Eq. 4a and 4b) yields four different exponential function coefficients that describe the magnetization. Three of these coefficients are positive while one of them is negative, indicating that M_{AZ} is relaxing as the sum of two exponential functions, while M_{BZ} is relaxing as the difference of two exponential functions. With the integration of the T_2 measurement, there is some signal separation and the result is an observed signal with four T_1-T_2 components, one of which has negative amplitude. In theory, fitting the two-dimensional data should reveal four components in the T_1-T_2 spectrum, for a two pool model. However, the non-negative least squares (NNLS) fitting technique that is common in these integrated measurements, and which is implemented in this thesis, prohibits this observation. This is in part due to the presence of a T_1-T_2 signal component that has negative amplitude. For this reason it is more likely that the NNLS analysis provides approximate T_1 values for each T_2 component.

The motivation behind this work is based on results from previous studies in edematous muscle [13,14]. In these studies a single concentration of λ-carrageenan was used to create edema. Both studies observed MET_2 as well as two-component diffusion characteristics with edematous muscle. Though these signal characteristics confirmed the use of a two-pool model when investigating inflammation in muscle tissue, it was unclear the effect of edema on T_1 in the tissue. It was unknown whether the amount of edema and compartmental exchange would allow the observation of MET_1. The goal of this study, then, was to investigate changes in both T_1 and T_2 over a range of tissue swelling, corresponding to various injection concentrations of λ-carrageenan. Knowledge of T_1 with edema will help prevent biasing of data by selecting an inappropriate value of TR in experiments focused on muscle at high fields. In addition, information about the changes in relaxation times might help describe the exchange process between intracellular and extracellular tissue compartments with muscle injury.

CHAPTER II

MATERIALS AND METHODS

II.1 Animal Model and Preparation

Female Sprague-Dawley rats (n=8, 201-242g, mean=223g) were used for all experiments per animal protocols approved by the Institutional Animal Care and Use Committee (IACUC) at Vanderbilt University. In order to induce edema, solutions of λ-carrageenan (Sigma Aldrich, St. Louis, MO, USA) were made by dissolving the solute in sterile saline (0.9% NaCl) in a 1 g per 100 mL solvent ratio for a 1.0% w/v solution and likewise for 0.5% w/v, 0.25% w/v, and 0.125% w/v solutions. Multiple concentrations of the λ-carrageenan solution were used to create a graded edema model that simulates various degrees of muscle injury and inflammation. Each rat was anesthetized with 2% isoflurane (Forane, Baxter Healthcare Corporation) and given a 0.1 mL subcutaneous injection of either a 1.0% w/v λ-carrageenan solution (n=2), 0.5% w/v solution (n=2), 0.25% w/v solution (n=2), or a 0.125% w/v solution (n=2) in the right hindlimb below the knee. The animals were then allowed to recover and rest. Each animal was observed once an hour post injection, up to the time of imaging, to monitor any change in behavior associated with the injury to the hindlimb. As indicated by a previous study [32], at least 6 hours were allowed before imaging for the level of fluid accumulation (edema) to reach a plateau.

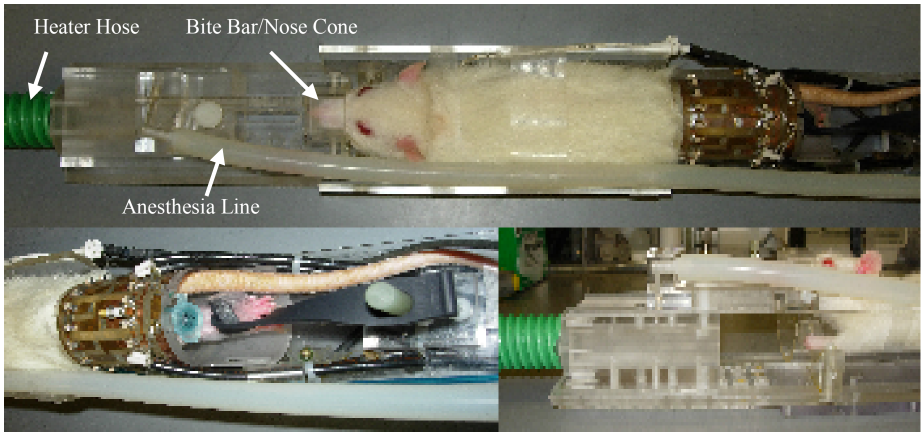

Figure II.1. Picture of experimental setup. (top) Animal positioned in cradle and RF coil. (bottom left) Feet are bound and stretched through center of the rf coil and water phantom is placed inside. (bottom right) Animal's head is secured by bite bar and anesthesia is delivered by integrated nose cone. Heater hose for warm air delivery can also be seen.

Prior to placing the animal in the magnet, the animal was anesthetized with isoflurane (2% induction and 1.5-2% maintenance) and placed in a customized cradle to allow for optimal placement of both legs in the RF coil. The cradle allowed the rat to lie prone while its head was secured by a custom bite bar/nose cone apparatus to ensure proper delivery of anesthesia and reduction of unwanted motion. The feet were bound together by a strap and stretched through the RF coil so that the region to be imaged was suspended in the center of the coil with the toes pointed inline with the coil. The strap was secured on the side of the coil opposite of the body. A picture of the setup can be seen in Fig. II.1. Respiration was monitored using a pneumatic pillow placed under the animal near the abdomen. Body temperature was monitored and maintained at 37°C by a stream of warm air directed at the animal. The use of smaller rats and a larger RF coil in this study, when compared to a previous study [14], allowed both hindlimbs to be imaged at the same time, providing the ability to simultaneously analyze edematous and healthy skeletal muscle in either limb.

II.2 MRI

Imaging was performed at 400 MHz on a 9.4T 21 cm horizontal-bore magnet equipped with a Varian Direct Drive console (Varian Inc, Palo Alto, CA, USA). Both of the rats' legs were positioned into a 38 mm diameter Litz coil (Doty Scientific, Columbia, SC, USA) for RF transmission and reception. In addition, a small $MnCl_2$ doped water phantom was placed in the coil with the legs to be imaged. The coil was then centered in the bore of the magnet and tuned and matched. To visualize the edematous muscle, a multi-slice fast spin-echo (FSE) sequence with a 40 mm by 40 mm field of view was used. From these scout images, a 2 mm thick axial slice was selected for further measurements. From the selected 2 mm slice, a rectangular volume of interest (VOI) was selected that encompassed the entire edematous hindlimb. A point-resolved spectroscopy (PRESS) sequence was used to manually shim the magnetic field over the VOI. Typical line widths were around 60 Hz for a ~ 20x15x10 mm^3 volume. Power calibration was then manually performed to optimize the 180° composite refocusing pulses in order to minimize errors in the T_2 measurements [36,37].

The integrated T_1-T_2 measurements were made with a multiple spin-echo (ME) single slice sequence at various repetition times (TR). The pulse sequence for the multiple spin-echo measurements can be seen in Fig. II.2. The second bracketed portion of the pulse sequence diagram represents the collection of echoes at late echo spacing. The collection of late echoes at longer echo spacing allows for a better characterization of long T_2 components that may be present in the tissue [38]. In this way if multiexponential relaxation is present, as has been shown with edema, one does not have to compromise the resolution of longer T_2 components by fixing the echo time at a shorter period in order to more accurately sample the short T_2 component.

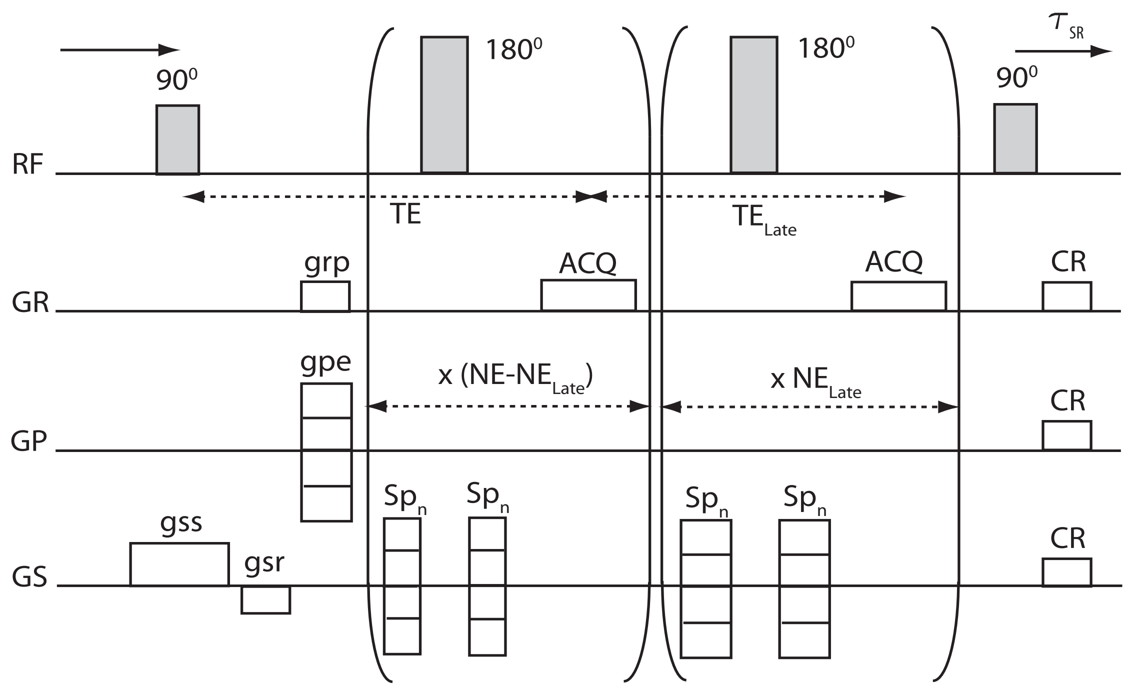

Figure. II.2. Pulse sequence diagram for the multiple spin-echo (ME) imaging sequence. RF, radio frequency; GR (read direction gradient); GP (phase direction gradient); GS (slice direction gradient); grp, read gradient preparation; gpe, stepped phase encode gradient; gss, slice select gradient; gsr, slice refocusing gradient; Sp_n, spoiler gradient for n^{th} echo; CR, crusher gradients; TE, echo time; TE_{Late}, echo spacing for late echoes; ACQ, acquisition; NE, number of echoes; NE_{Late}, number of late echoes; τ_{SR}, saturation recovery time.

There are several features of this particular pulse sequence that serve to optimize the T_1 and T_2 measurements. Each 180° refocusing pulse is actually a composite pulse consisting of three pulses $90°_x$-$180°_y$-$90°_x$. The composite pulse is used to reduce the effects of imperfect refocusing due to B_1 field inhomogeneities and resonance offset effects [39]. Surrounding each non-selective 180° refocusing pulse is a pair of spoiler gradients used to eliminate spurious contributions from unwanted coherence pathways. The spoiler gradient amplitudes satisfy the conditions presented by Crawley and Henkelman [40]. The amplitudes of the spoiler gradients for the early echoes were modulated in a descending fashion with an increase in echo number. The spoiler amplitudes in the acquisition of late echoes were modulated in a similar fashion though these gradient amplitudes were larger than those corresponding to earlier echoes. The sequence also employed an add/subtract two step phase cycling for reducing unwanted magnetization and stimulated echoes [41]. At the end of the sequence is an additional 90° saturation pulse followed by crusher gradients in all directions to define the start of the saturation recovery period.

For the ME measurements, 36 echoes were collected, 30 of these echoes were collected at TE=10 ms, while the remaining six echoes were collected at TE_{late}=50 ms. Thirteen TR times were spaced pseudo-logarithmically between 875 ms and 12s. The remaining imaging parameters were as follows: FOV = 40x40 mm^2, 64x64 samples, spectral width = 35.7 kHz, acq. time = 1.79 ms, and NEX = 2. The total imaging time was 1 hour 40 minutes.

II.3 Parameter Definitions

With similar parameters being extracted from both the acquired T_1-T_2 data and from the exchange model, some definitions are needed to avoid confusion. The apparent values for the parameters in model I are obtained from the T_1-T_2 spectrum created from a non-negative least squares (NNLS) fitting of the acquired 2D echo magnitude data as described in the next section. Model II is a two pool exchange model similar to the model in Fig. 1.1. In this model the Bloch-McConnell equations are solved for various amounts of swelling and the resulting two-dimensional echo magnitude data is analyzed in an NNLS sense to extract the apparent values for the parameters. The same NNLS analysis in model I is used in model II. The parameters and their description for each model can be seen in Fig. II.3.

Model I		Model II	
Parameter	Description	Parameter	Description
$\hat{T}_{1A,I}$	Apparent longitudinal relaxation in the fast relaxing compartment	$\hat{T}_{1A,II}$	Apparent longitudinal relaxation in the fast relaxing compartment
$\hat{T}_{1B,I}$	Apparent longitudinal relaxation in the slow relaxing compartment	$\hat{T}_{1B,II}$	Apparent longitudinal relaxation in the slow relaxing compartment
$\hat{T}_{2A,I}$	Apparent transverse relaxation in the fast relaxing compartment	$\hat{T}_{2A,II}$	Apparent transverse relaxation in the fast relaxing compartment
$\hat{T}_{2B,I}$	Apparent transverse relaxation in the slow relaxing compartment	$\hat{T}_{2B,II}$	Apparent transverse relaxation in the slow relaxing compartment
$M_{0A,I}$	Total magnetization in the fast relaxing compartment in normal muscle	$M_{0A,II}$	Total magnetization in the fast relaxing compartment in normal muscle
$M_{0B,I}$	Total magnetization in the slow relaxing compartment in normal muscle	$M_{0B,II}$	Total magnetization in the slow relaxing compartment based on the amount of swelling
$\hat{\rho}_{A,I}$	Apparent volume fraction in the fast relaxing compartment	$\hat{\rho}_{A,II}$	Apparent volume fraction in the fast relaxing compartment
$\hat{\rho}_{B,I}$	Apparent volume fraction in the slow relaxing compartment	$\hat{\rho}_{B,II}$	Apparent volume fraction in the slow relaxing compartment
		P_k	Ratio of the total integrated edematous muscle signal from the T_1-T_2 spectrum to the integrated normal muscle signal
		τ_A	Mean water residence time from the fast relaxing compartment
		τ_B	Mean water residence time from the slow relaxing compartment

Figure II.3. List of model parameters and associated descriptions. Parameters in model I are obtained from the T_1-T_2 spectrum created from a NNLS fitting of the acquired 2D echo magnitude data. Model II is a two pool exchange model similar to the model in Fig. 1.1

When the apparent parameters are discussed for normal muscle tissue or in a general sense, they appear without the subscripts A and B used to denote the two pools. The fitted values for the apparent relaxation times are indicated as $\hat{T}_{1A}$, $\hat{T}_{1B}$, $\hat{T}_{2A}$, $\hat{T}_{2B}$, without the additional subscript indicating the model.

In the graded edema model presented in this thesis, the muscle tissue experiences various amounts of edema and therefore various degrees of swelling in the intracellular and extracellular compartments. The parameter P_k is an indicator of the amount of swelling in which the subscript k = 1, 2, 3, or 4. The values one through four represent the number of the experiment, where each experiment corresponds to a different injection concentration (i.e. experiment 1 = 0.125 % w/v, experiment 2 = 0.25% w/v, etc.). Attempts have been made to measure the intracellular volume fractions in healthy skeletal muscle [42,43]. The value of $M_{0A,II}$ used in this study based on the literature was 0.89 [44]. The value of $M_{0B,II}$ is dependent on P_k and was calculated by the following equation

$$M_{0B,II} = P_k - M_{0A,II} \qquad \text{(Eq. 7)}$$

The values of both $M_{0A,II}$ and $M_{0B,II}$ are normalized to the sum of the two magnetizations for use in the exchange model. The value of τ_A used in the exchange model was 1.1s, as found by Landis *et al*. for rat skeletal muscle [44]. The value of τ_B was calculated by Eq. 8.

$$\tau_B = \frac{M_{0B,II}}{M_{0A,II}} \cdot \tau_A \qquad \text{(Eq. 8)}$$

As an input to the exchange model, values for R_{1B} and R_{2B} after swelling were approximated by a linear model

$$R_i = R_{i,0} + r_i \frac{N}{V} \qquad \text{(Eq. 9)}$$

where $R_{i,0}$ is the relaxation rate of free water at a particular temperature, r_i is the relaxivity (s^{-1}/concentration), N is number of macromolecules in the solution, and V is the volume. If R_i and $R_{i,0}$ are known when the extracellular space is not swollen, then the 2nd term on the right hand side of Eq. 9 can be determined and can be used to find the value of R_i for any relative volume increase. For measures of transverse relaxation, the $R_{2,0}$ term can usually be ignored because it is much smaller than R_2. In this linear model and in the model used for the Bloch-McConnell simulations $R_{1,0}$, the longitudinal relaxation rate of free water at 37°C, is ~ $0.192s^{-1}$ or $T_{1,0}$=5.20s [45].

II.4 Data Analysis

Once a set of multiple spin-echo images were collected, the k-space data were zero-padded to a 128 x 128 matrix and transformed. Regions of interest (ROI) were manually selected in healthy muscle, edematous muscle, in the water phantom, and in the background signal. The healthy muscle ROI was selected on the hindlimb without edema in approximately the same location as the edematous muscle ROI. Special care was taken when selecting the edematous muscle region to avoid areas of pooling fluid or areas of subcutaneous fat. Areas of edema were selected that appeared to be feathered in a roughly uniform manner across the ROI. The ROIs selected were kept fairly small, ranging only from 20 to 30 pixels in size. Mean echo magnitudes were extracted from the 36 x 13 image set. The image data were corrected for Rician noise [46], while the standard deviation of the noise was estimated from the background ROI and corrected for Rayleigh bias. For a single TR, decay curves were plotted, for the purpose of visualization, for the selected ROIs. At this same TR, the ROI based echo magnitudes were transformed into a T_2 spectrum using a process described by Whittall and MacKay [47].

The ME echo magnitudes were represented by the two-dimensional summation of the product of two exponential functions

$$M(\tau_{SR}, TE) = \sum_{k=1}^{N_2} \sum_{l=1}^{N_1} S_{kl} (1 - \alpha \cdot \exp(-\tau_{SR} / T_{1k})) \exp(-TE / T_{2l}) \qquad \text{(Eq. 10)}$$

where S_{kl} is the integrated T_1-T_2 spectral intensity and α is a scalar that accounts for imperfect saturation and ranges from 0 to 2. The value of α is estimated by fitting the magnitude of the first echo at each TR to a monoexponential recovery with unknown initial conditions:

$$M(TR) = M_0 (1 - \alpha \cdot \exp(-TR / T_1)) \qquad \text{(Eq. 11)}$$

where M_0, T_1, and α are unknown. The T_1-T_2 spectrum can then be estimated from Eq. 10 using a NNLS fitting routine [48].

In the NNLS analysis, a regularization parameter, μ, was incorporated to help create a more continuous distribution of relaxation times and to increase the stability of the solution. The value of μ was selected to help satisfy additional constraints while attempting to reduce the χ^2 misfit. Additional constraints were added to minimize the energy in the curvature based on the second derivative in each direction.

II.5 Inter-compartmental Exchange Simulations

As indicated in the introduction, exchange between tissue compartments will have an effect on the values of the relaxation times and volume fractions that are observed in the integrated T_1-T_2 measurements. To provide a comparison for the observed parameters extracted from the T_1-T_2 measurements, a two-pool model was created and the Bloch-McConnell equations (Eqs. 4a and 4b) were solved for longitudinal and transverse magnetization with compartmental swelling taken into consideration. The exchange model is similar to that seen in Fig. I.1.

In the exchange model, the relaxation times for the two pools served as the free parameters. Initial input values for the relaxation times used in this model were based on $\hat{T}_{1,I}$ and $\hat{T}_{2,I}$. The value of P_k was used as an indicator of the amount of swelling, to create the two-dimensional data from simulation of the Bloch-McConnell equations and the model parameters. The two-dimensional echo magnitude data, based on the exchange model, were then compared to the observed two-dimensional echo magnitude data through a non-linear least squares fitting process. The data were fitted in a non-linear sense using a Trust-Region algorithm implemented with the *lsqnonlin* function in MATLAB (Natick, MA, USA). A cost function was created that aimed to minimize the root mean squared error between the model and observed data. Fitted parameters were obtained for each of the compartmental relaxation times. Numerical estimates of the

Jacobian and residuals to the fit were used, with the *nlparci* function in MATLAB, to estimate uncertainty in the fitted parameters by means of 95% confidence intervals.

CHAPTER III

RESULTS

In this study edema was created in the right hindlimb for all of the rats. Fig. III.1 shows a typical fast spin echo image of both a healthy and injured rat hindlimb. The edema induced in this image was a result of a 0.5% w/v injection of λ-carrageenan solution. When compared to the control, the increase in signal intensity in the lateral portion of the right hindlimb is apparent. The ability to image both hindlimbs simultaneously allowed for the analysis and comparison of normal muscle tissue from both the healthy and injured limb.

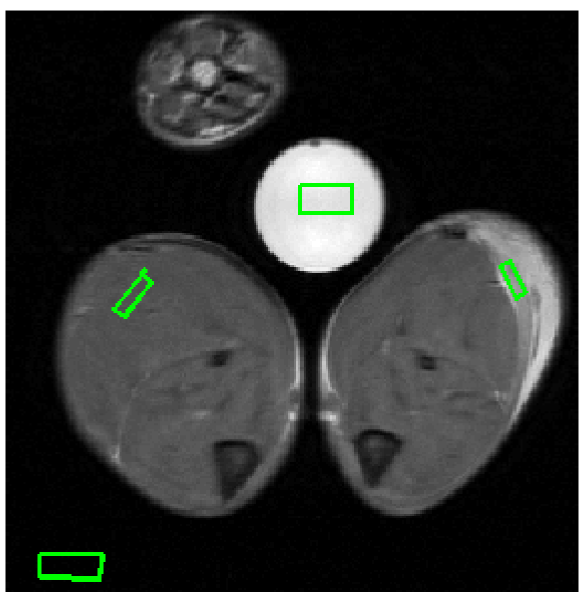

Figure III.1. Example of a fast spin echo (FSE) image of a healthy rat hindlimb (left) and a rat hindlimb with edema (right). Image parameters: 256 x 256, 40 x 40 mm^2, TR = 2000ms, TE = 20 ms.

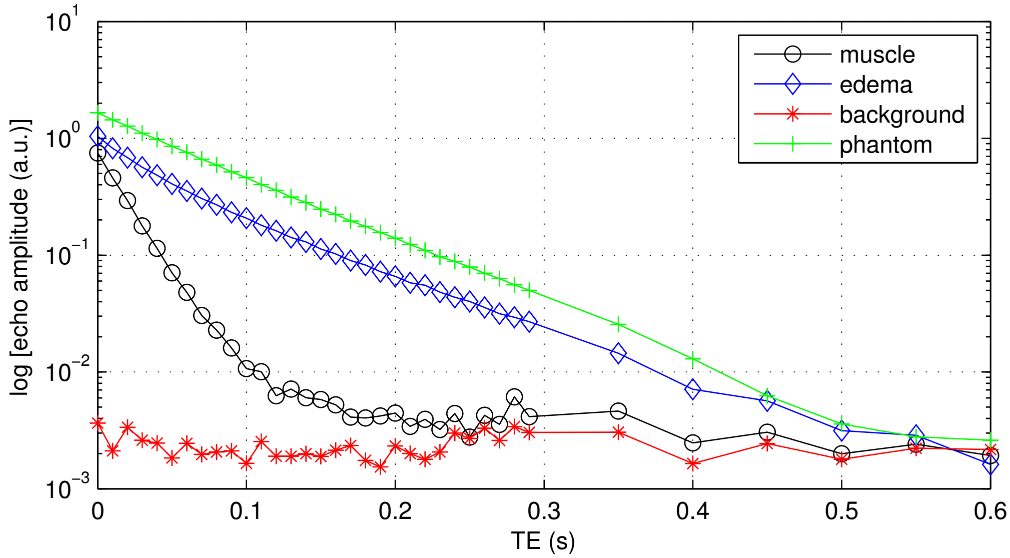

Figure III.2. Plot of logarithmic decay curves of example data acquired from selected ROIs.

It can be seen from Fig. III.2 that the signal from the healthy muscle tissue is short lived and the decay is approximately linear prior to an echo time of about 100 ms. Therefore, it appears the decay of the normal muscle tissue can be described as monoexponential. After this time the signal decays towards the noise floor where it begins to follow a pattern similar to that of the background signal. Alternatively, the decay curve for the region of edema has a curvature that is indicative of multiexponential T_2 decay. As expected, the decay curve for the homogeneous water phantom is linear, representing a single T_2 value. From these plots it is easy to see the multiple echo sampling scheme as well as the signal amplitudes at late echoes.

Fig. III.3 shows the T_2 spectra, normalized to healthy muscle, of the two animals subject to a 1.0% w/v injection in a region of (a) normal muscle and (b) edematous muscle. In comparison of the T_2 spectra, it can be seen that the normal muscle has a peak around 20 ms while the T_2 spectra for edematous muscle have two peaks, $\hat{T}_{2A,I} \approx 27$ ms and $\hat{T}_{2B,I} \approx 105$ ms.

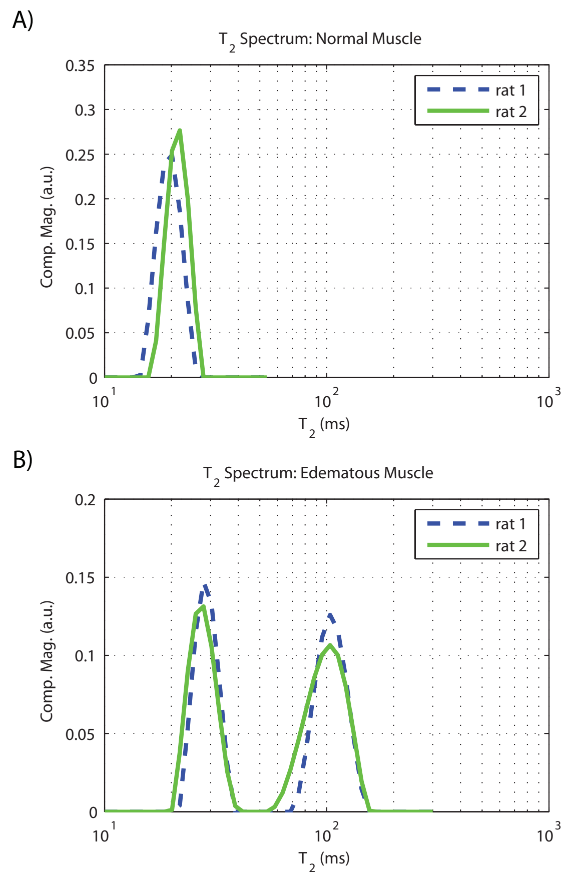

Figure III.3. Normalized T_2 spectra of A) normal muscle and B) edematous muscle for two rats subject to a 1.0% w/v injection.

As has been demonstrated in previous studies at lower field strengths [13,14], the result of inflammation/edema in rat skeletal muscle creates a bi-exponential T_2 decay that results in two distinct T_2 components, with the short-lived T_2 component postulated to correspond to intracellular muscle water and the long-lived T_2 component corresponding to extracellular muscle water. Fig. III.3b shows that $\hat{T}_{2A,I}$ has shifted to a value that is larger than that of the single component in normal muscle. The appearance of the $\hat{T}_{2B,I}$ component reflects the swelling of the extracellular space.

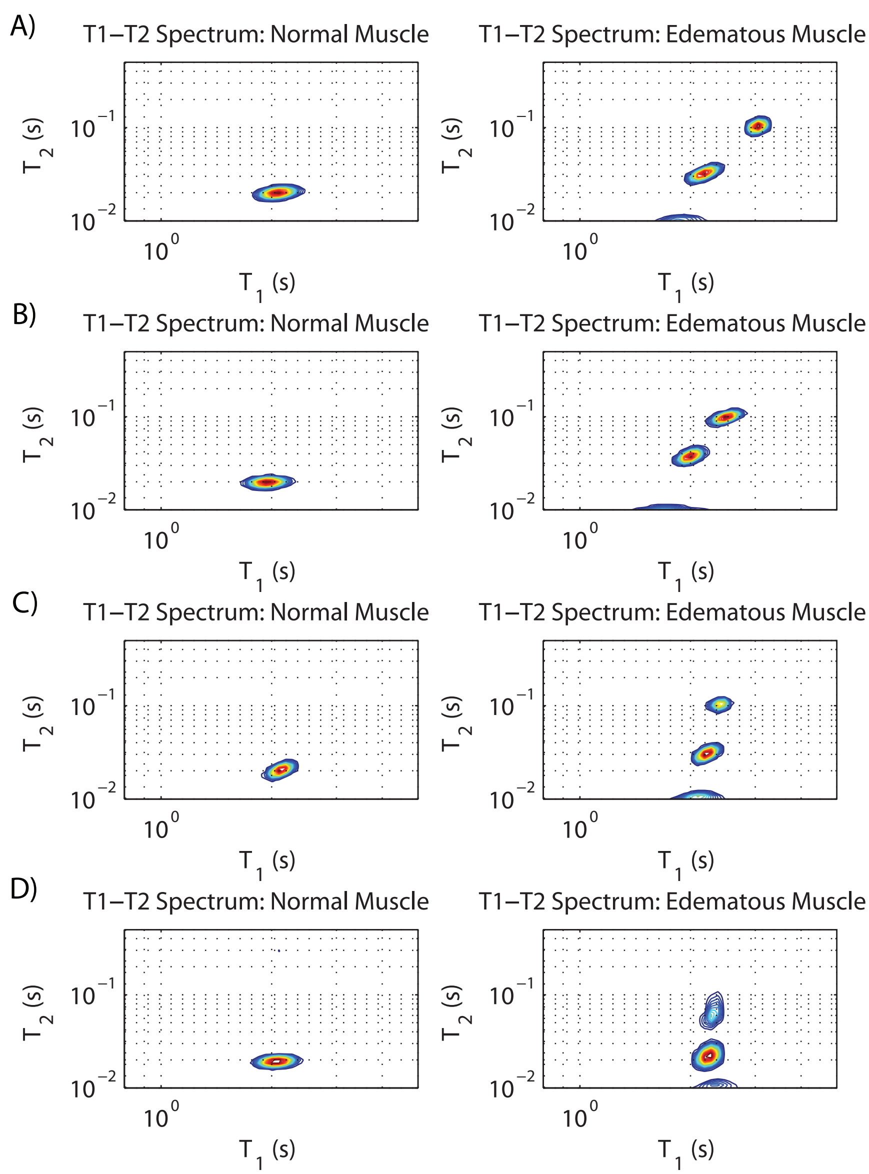

Figure III.4. T_1-T_2 spectra of normal muscle and edematous muscle for a 1.0% w/v injection (A), 0.5% w/v (B), 0.25% w/v (C), and 0.125% (D).

Fig. III.4 shows two-dimensional plots of single T_1-T_2 spectra in edematous and normal muscle. The plots reveal that edematous muscle displays two main T_2 components, each with its own distinct T_1 value. This indicates the presence of both multiexponential T_2 (MET_2) and multiexponential T_1 (MET_1). T_1-T_2 plots were created for the aforementioned ROIs in all eight animals. In the T_1-T_2 measurements the average SNR per pixel in edematous muscle was 484 ± 109 (range 340-648). If more than two components were present as a result of the NNLS analysis, the two largest components (based on volume fractions) were selected as representing the edematous muscle. In this case $\hat{\rho}_{A,I}$ and $\hat{\rho}_{B,I}$, were recalculated based on two components alone. In certain cases the smaller components that were present represented up to ~20% of the total signal. The data from the integrated measurements were tabulated and can be seen in Table III.1.

Table III.1. Calculated parameters for normal and edematous muscle from integrated T_1-T_2 measurements at various injection concentrations

	1.0% w/v injection			**0.5% w/v injection**		
	$\hat{\rho}_I$	$\hat{T}_{2,I}$ (ms)	$\hat{T}_{1,I}$ (s)	$\hat{\rho}_I$	$\hat{T}_{2,I}$ (ms)	$\hat{T}_{1,I}$ (s)
Normal	1.0	19.4±0.8	2.08±0.01	1.0	19.8±0.1	2.05±0.14
$Edema_A$	0.57±0.03	29.0±4.7	2.27±0.12	0.58±0.04	31.5±8.9	2.22±0.30
$Edema_B$	0.43±0.03	109.6±8.8	2.99±0.09	0.42±0.04	99.7±1.6	2.61±0.16
Phantom	1.0	78.4±1.6	1.36±0.10	1.0	81.0±2.4	1.34±0.08

	0.25% w/v injection			**0.125% w/v injection**		
	$\hat{\rho}_I$	$\hat{T}_{2,I}$ (ms)	$\hat{T}_{1,I}$ (s)	$\hat{\rho}_I$	$\hat{T}_{2,I}$ (ms)	$\hat{T}_{1,I}$ (s)
Normal	1.0	20.7±0.4	2.16±0.05	1.0	19.8±0.8	2.17±0.02
$Edema_A$	0.69±0.02	27.3±4.9	2.29±0.09	0.73±0.01	23.9±2.3	2.34±0.11
$Edema_B$	0.31±0.02	88.5±20.1	2.43±0.03	0.27±0.01	71.7±5.0	2.22±0.01
Phantom	1.0	83.4±1.0	1.28±0.05	1.0	79.1±3.3	1.28±0.04

Mean ± SD across animals. Apparent spin density values, $\hat{\rho}_I$, are given as fractional values for each ROI.

Table III.1 reveals several noteworthy items. The normal muscle tissue exhibits monoexponential $\hat{T}_{1,I}$ and $\hat{T}_{2,I}$ values. The values of $\hat{T}_{1A,I}$ and $\hat{T}_{2A,I}$ are slightly larger than the values of $\hat{T}_{1,I}$ and $\hat{T}_{2,I}$ in normal muscle. However, $\hat{T}_{1B,I}$ and $\hat{T}_{2B,I}$ are much longer than the $\hat{T}_{1,I}$ and $\hat{T}_{2,I}$ values found in normal muscle. As Fig. III.5a reveals, $\hat{T}_{1B,I}$ increases with an increase in size. The increase in compartment size is a result of the increase in the amount of edema as larger concentrations of λ-carrageenan were injected. Drawing a similar conclusion, as the injection concentration of λ-carrageenan increased, so to did the value of $\hat{T}_{1B,I}$. This relationship can be seen in Fig. III.5b. It may be postulated that at a certain injection concentration $\hat{T}_{1B,I}$ will reach a plateau and will be similar to that of free water.

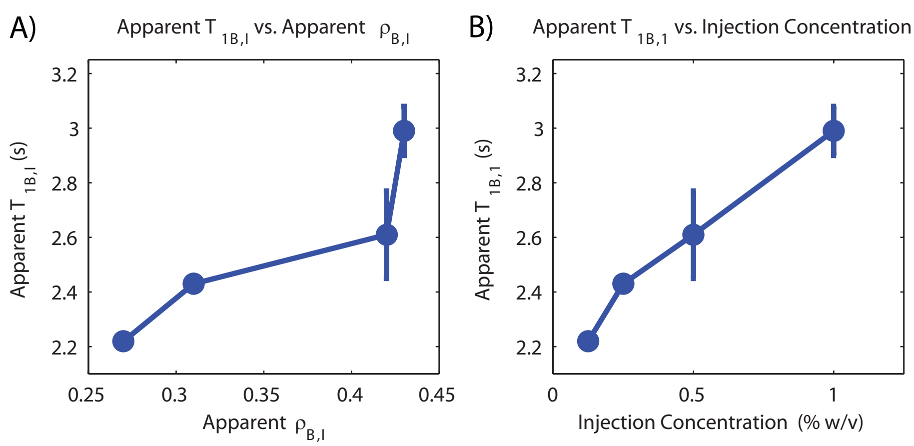

Figure III.5. A) Plot of $\hat{T}_{1B,I}$ for corresponding values of $\hat{\rho}_{B,I}$. B) Plot of $\hat{T}_{1B,I}$ for each injection concentration of λ-carrageenan.

Exchange Simulations

Analysis of the exchange model and subsequent fitting using the aforementioned echo magnitude method resulted in several observations. As an input to this model, the value of P_k was found to be 1.05, 1.12, 1.17, and 1.22 as a result of averaging across animals. The results of this fitting method are seen in Table III.2.

Table III.2. Fitted parameter values and confidence intervals for compartmental relaxation times

Parameter	Fitted Value	Confidence Interval
$\hat{T}_{1A}$ (s)	2.16	2.07 – 2.25
$\hat{T}_{1B}$ (s)	2.80	2.07 – 4.36
$\hat{T}_{2A}$ (ms)	29.3	29.1 – 29.5
$\hat{T}_{2B}$ (ms)	71.6	70.5 – 72.8

The fitted values in Table III.2 represent the relaxation times for each compartment that, when included in the Bloch-McConnell simulations, best describe the observed data with the given values of P_k. We note that the 95% confidence intervals for $\hat{T}_{2A}$ and $\hat{T}_{2B}$ are quite tight and the fitted value for $\hat{T}_{1A}$ is only slightly larger than the average value of $\hat{T}_{1,I}$ in normal muscle, 2.11 s. The confidence interval for $\hat{T}_{1B}$ is larger than that for $\hat{T}_{1A}$ suggesting that the model is not as sensitive to the changes in longitudinal relaxation as the long-lived compartment changes in size. Figure III.6 shows examples of the two-dimensional echo magnitude data from edematous muscle at each of the injection concentrations. The solid lines represent echo magnitude data from the exchange model at each injection concentration based on the appropriate value of P_k.

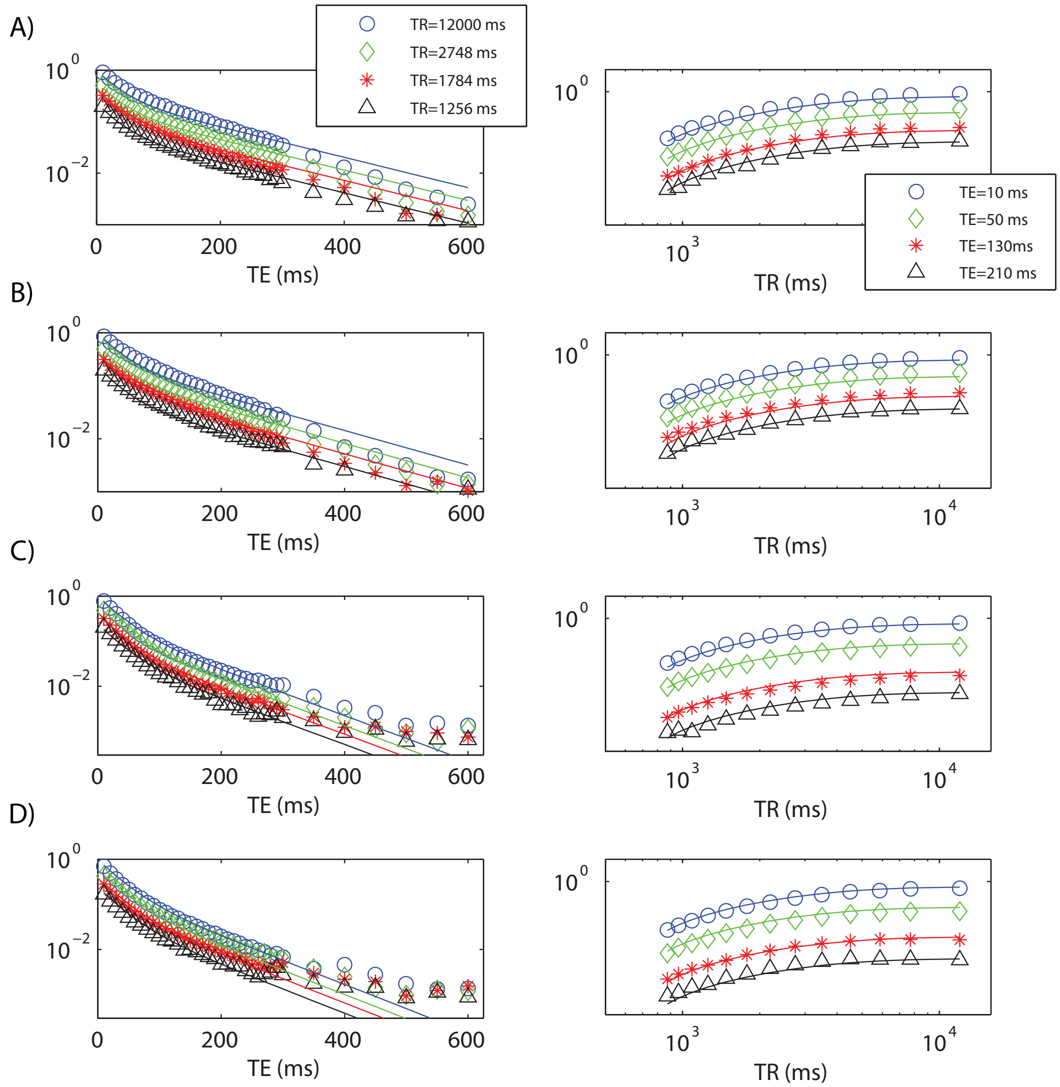

Figure III.6. Sample of variable TR ME echo magnitudes for edematous muscle at A) 1.0% w/v injection, B) 0.5% w/v injection, C) 0.25% w/v injection, and D) 0.125% injection. (left) Log-magnitude plots of echo decays at four different TR times as a function of TE. (right) Log-log plots of echo magnitude vs. TR at four different echo times.

Based on the acquired data and the model data, the residuals were plotted for each of the injection concentrations. These plots can be seen in Fig. III.7.

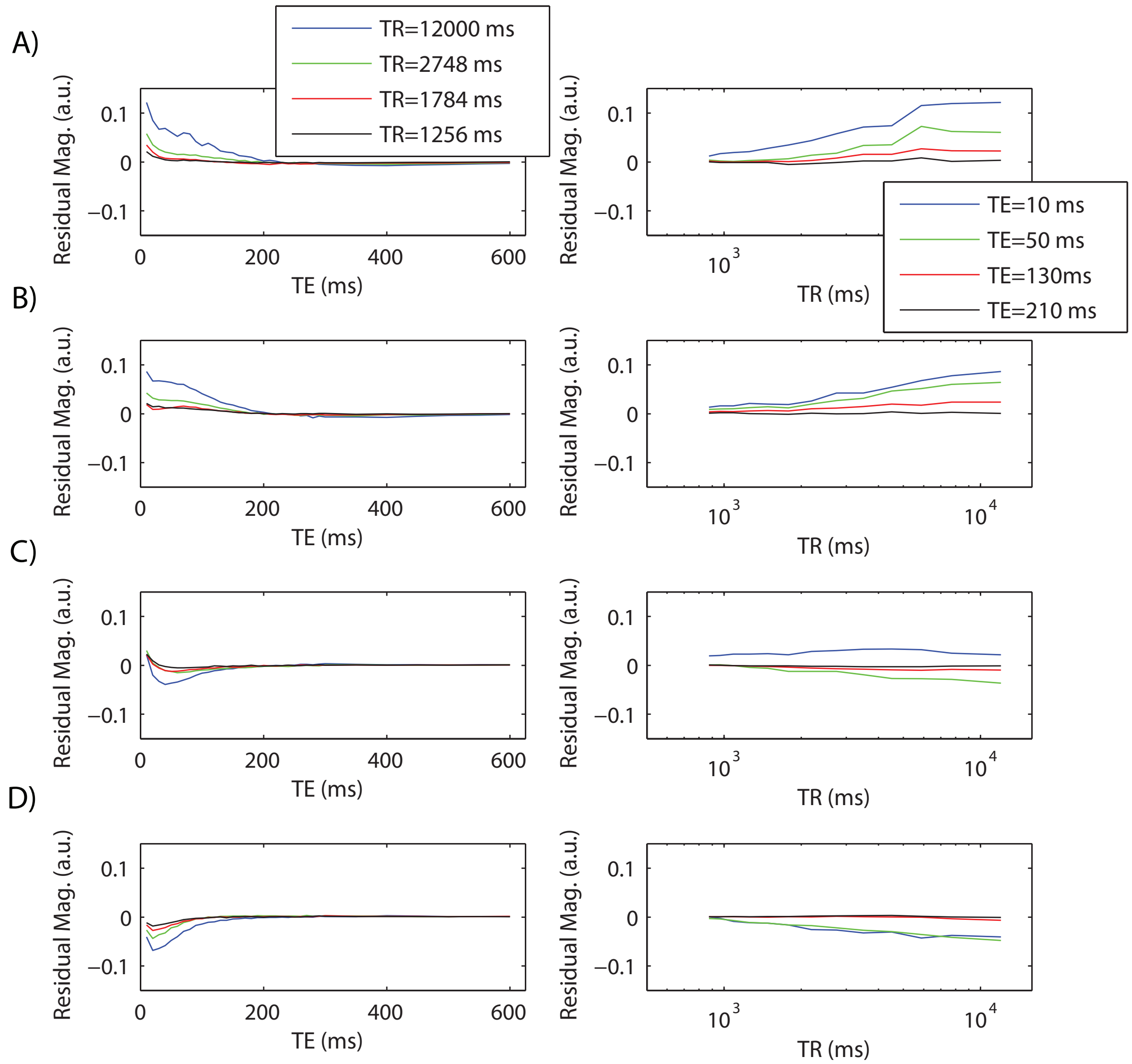

Figure III.7. Plot of the residuals based on acquired 2D echo magnitude data and model data for edematous muscle at A) 1.0% w/v injection, B) 0.5% w/v injection, C) 0.25% w/v injection, and D) 0.125% injection. Residuals correspond to plots in Fig. III.6.

If the fitted values for each of the relaxation parameters are input, as initial values, into the original exchange model, two-dimensional data is created that can be analyzed in a NNLS sense to obtain a T_1-T_2 spectrum at each injection concentration. The resulting spectra can be seen in Fig. III.8.

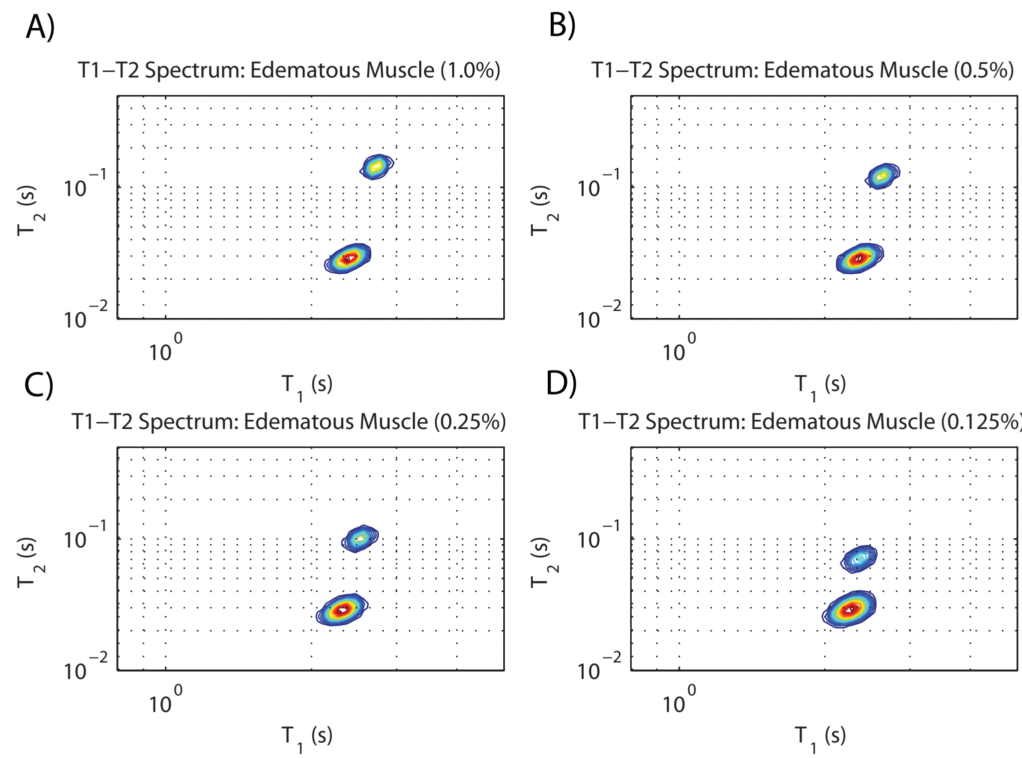

Figure III.8. Plot of T_1-T_2 spectra from an NNLS analysis of simulated model data with fitted parameters. A) 1.0% (P_4=1.22), B) 0.5% (P_3=1.17), C) 0.25% (P_2=1.12), and D) 0.125% (P_1=1.05).

Just as with the observed data, creation of the T_1-T_2 spectra allows the extraction of $\hat{T}_{1A,II}$, $\hat{T}_{1B,II}$, $\hat{T}_{2A,II}$ and $\hat{T}_{2B,II}$ as well as $\hat{\rho}_{A,II}$ and $\hat{\rho}_{B,II}$. For the spectra created with the model and fitted parameters, the calculated parameters can be seen in Table III.3.

Table III.3. Calculated parameters for edematous muscle from the Bloch-McConnell simulations of the exchange model

Concentration	$\hat{\rho}_{A,II}$	$\hat{T}_{2A.II}$ (ms)	$\hat{T}_{1A,II}$ (s)	$\hat{\rho}_{B,II}$	$\hat{T}_{2B,II}$ (ms)	$\hat{T}_{1B,II}$ (s)
1.0%	0.68	28.8	2.39	0.32	144.0	2.72
0.5%	0.71	28.8	2.36	0.29	122.3	2.63
0.25%	0.74	28.9	2.32	0.26	100.7	2.52
0.125%	0.78	29.2	2.26	0.22	71.0	2.36

From the parameters in Table III.3 one notices that the values of $\hat{\rho}_{B,II}$ are not as large as those in the observed measurements, especially for the case of the 1.0% and 0.5% injection concentrations. Accordingly, $\hat{T}_{1B,II}$ in the case of a 1.0% injection is smaller than what was found *in vivo*. In addition, $\hat{T}_{2B,II}$ is overestimated when compared to $\hat{T}_{2B,I}$ in the 1.0%, 0.5%, and 0.25% concentrations.

CHAPTER IV

DISCUSSION

IV.1 Normal Skeletal Muscle

The region of healthy skeletal muscle exhibits both monoexponential T_1 and T_2 relaxation. The value of $\hat{T}_{2,I}$, 19.9 ± 0.7 ms, that was recorded from the integrated T_1-T_2 measurements (n=8) is comparable to those found at 7T in rat hindlimb [14], T_2 = 23.7 ± 1.0 ms, and in rat paw [20], T_2 = 20.2 ± 1.0 ms. To the author's knowledge, T_1 and T_2 values for *in vivo* rat skeletal muscle at 9.4T have yet to be published. Following the trend of an increase in T_1 in tissue with an increase in field strength, the value of $\hat{T}_{1,I}$ that was found for normal skeletal muscle, $\hat{T}_{1,I}$ = 2.11 ± 0.08 s, was larger than values of T_1 presented in studies at lower field strengths [49-51].

Chen *et al*. performed *in vivo* measurements on rat muscle at 4.85T and found muscle to have a single T_1 value of 1.903 ± 0.030 s and a T_2 of 24.3 ± 0.5 ms [49]. Both Gold *et al*. and Duewell *et al*. compared T_1 and T_2 relaxation times of human skeletal muscle at 1.5T vs. 3.0T and 4.0T, respectively [50,51]. These studies showed an increase in T_1 and slight decrease in T_2 with increasing field strength. Duewell reported a T_1 value of 1.830 ± 0.173 s at 4T while T_2 decreased from 31.0 ± 0.001 ms at 1.5T to 26.0 ± 0.001 ms at 4.0T. In the same manner, the T_2 reported here at 9.4T was slightly smaller when compared with the monoexponential T_2 reported by Fan at 7.0T [14].

Despite the finding that normal skeletal muscle displays monoexponential T_1 and T_2 there are some studies that have shown normal skeletal muscle to exhibit multiexponential T_2, though few studies exist *in vivo* [10,11,19]. In particular, the study by Saab *et al*. [19] showed multiexponential T_2 and T_1 in *in vivo* skeletal muscle with the use of a single-voxel CPMG imaging sequence with very high SNR. The lower SNR of the integrated measurements, as compared to a single voxel measurement, could be one explanation as to why multiexponential relaxation was not observed in healthy muscle. Simulations of the exchange model for normal muscle with noise added (corresponding to the mean SNR in the *in vivo* measurements) produced only a single T_1-T_2 component. As is seen in Fig. III.4, the ROI analysis with ME measurements, consistently produced only monoexponential T_1 and T_2 values in healthy rat skeletal muscle.

IV.2 Edematous Skeletal Muscle

A ME measurement at a single TR revealed that edematous skeletal muscle exhibits biexponential T_2 relaxation, a finding consistent with previous studies that implemented a similar acute edema model [13,14]. What was of interest was the finding that each individual T_2 component also had a distinct T_1 relaxation component, confirming MET_1 in edematous muscle. By injecting the hindlimb with various concentrations of λ-carrageenan solution it was postulated that the volume fraction of the intracellular and extracellular compartments in muscle would change with the increase or decrease of edema.

As is seen in Table III.1 the value of $\hat{\rho}_{A,I}$ and $\hat{\rho}_{B,I}$, at a 1% w/v injection, displayed closer to a 60%-40% distribution. In this case, $\hat{T}_{1A,I}$, thought to correspond to intracellular muscle water, had a mean value of 2.27 ± 0.12 s while $\hat{T}_{1B,I}$, thought to correspond with extracellular muscle water, had a mean value of 2.99 ± 0.09 s. Ababneh *et al.* showed that a 2% w/v injection of λ-carrageenan resulted in signal fractions of 47% for the short-lived component and 53% for the long-lived component [13]. Based on this observation it seems that the apparent volume fractions presented here are feasible. It may be postulated that at a certain injection concentration, the extracellular space may become limited in the size to which it can swell.

For an injection concentration of 0.5% w/v, there was only a slight decrease in $\hat{\rho}_{B,I}$ over the previous measurement at 1% w/v, but $\hat{T}_{1B,I}$ decreased to a mean value of 2.61 ± 0.16 s. For an injection of 0.25% w/v a larger change was seen in $\hat{\rho}_{B,I}$ with a decrease to 31%. Just as before, the corresponding $\hat{T}_{1B,I}$ also decreased, to a mean value of 2.43 ± 0.03 s. For the lowest concentration injected, 0.125% w/v, the results were somewhat unexpected. $\hat{\rho}_{B,I}$ continued to decrease to 27% and with it, the mean $\hat{T}_{1B,I}$ also decreased to 2.22 ± 0.01 s. However, the mean $\hat{T}_{1A,I}$ increased to 2.34 ± 0.11 s. This abnormal increase in $\hat{T}_{1A,I}$ might be a result of the measurements made with a smaller volume of edema, at a lower injection concentration, and the effect of the NNLS analysis on these measurements in the presence of compartmental exchange (as described in the introduction).

For all amounts of edema, the value of $\hat{T}_{1A,I}$ was slightly longer than the $\hat{T}_{1,I}$ observed in normal muscle. This is consistent with the trend seen with $\hat{T}_{2A,I}$ when compared to the $\hat{T}_{2,I}$ of healthy muscle. The slight increase in relaxation time could be attributed to intracellular swelling. Though the effect of λ-carrageenan does produce swelling in the tissue early on, extensive changes due to muscle necrosis may not appear until much later. Radhakrishnan *et al*. showed that a 0.1 ml injection (with a concentration as high as 3% w/v) produced mild hemorrhaging, edema, and minimal inflammatory infiltrates (i.e. neutrophils) 4hrs after injection, though myonecrosis did not appear till 24 hrs post injection [52]. Knowledge of changes in relaxation parameters at more advanced stages of inflammation and necrosis might be used to supplement the information provided in this acute model to form a more comprehensive method for quantifying muscle injury.

IV.3 Effects of Exchange

As previously indicated, exchange between tissue compartments will have an effect on the values of the relaxation times and volume fractions that are observed in the integrated measurements. This presents a complicating factor when interpreting the two-dimensional data. Based on our observations in normal muscle, we can use $T_1 = 2.1$s as an input to Eq. 9 to help determine the value of T_1 with swelling. For example, if the extracellular space swells by a factor of 4, we would expect the T_1 of that space to increase to 3.80 s according to Eq. 9. However, this is not the case, possibly because we have not included the effect of exchange that may be occurring *in vivo*. The linear model in Eq. 9 is a relatively simple model and may overestimate T_{1B} due to a variety of unknown factors.

From the observed parameter values in Table III.1 it can be concluded that $\hat{T}_{1B,I}$ does in fact increase monotonically with an increase in injection concentration and relative size. The same trend is also seen on the scale of T_2. When Fig. III. 8 is compared to Fig. III. 4 the general trend described above can be seen in the spectra extracted from the model; however, the magnitude of change in $\hat{\rho}_{B,II}$ extracted from the exchange model is smaller, most notably for the cases of 1.0% and 0.5% injection concentrations. Across all levels of edema, a difference of 10% in $\hat{\rho}_{B,II}$ was calculated from the fitted model, as compared to a 16% difference in $\hat{\rho}_{B,I}$. In addition, the values of $\hat{T}_{2B,II}$ were somewhat overestimated by the simulations.

For ease of analysis, the exchange model presented in this thesis assumed that all of the swelling occurred in the extracellular space. As was briefly mentioned, it is possible that some intracellular swelling occurs concurrently to the extracellular swelling. This might provide an explanation for the discrepancies in values of $\hat{T}_{1A,I}$ when compared to the exchange model, and helps explain why the value of $\hat{T}_{2A,II}$ only changes slightly with a change in edema. The residuals plotted in Fig. III.7 based on the data in Fig. III. 6 show that at longer echo times, past TE=150 ms, the exchange model estimates the observed data relatively well. At shorter echo times however, the model underestimates the observed data for injection concentrations of 1.0% w/v and 0.5% w/v, and overestimates the observed data for 0.25% w/v and 0.125% w/v concentrations. These discrepancies between the model and observed data might be a result of physiological processes occurring with inflammation that may not be accounted for in the model.

The observation of MET_1 and MET_2 with edema provides some indication that the exchange rates are not fast compared to the longitudinal relaxation rates. On a T_1 time scale, the system may have yet to reach the slow exchange limit; however, this may not be the case on a T_2 time scale. As has been previously discussed, the accuracy of the observed T_1 values are not only affected by the exchange rates but also by the NNLS analysis. This may help explain some of the differences between the parameter values extracted from the model data, and those extracted from the acquired data *in vivo*.

In the study by Landis *et al.*, they showed that τ_A can be calculated for a two-site exchange model by

$$\tau_A^{-1} = P\left(\frac{A}{V}\right) \qquad \text{(Eq. 10)}$$

where P is the diffusional permeability coefficient of the compartmental wall, A is its surface area, and V is the volume of the intracellular compartment. If the muscle cell is modeled as an infinitely long cylinder, the ratio of A/V can be approximated by 2/r, where r is the cylinder radius. It has been reported that the average value of r for rat calf skeletal muscle cells is 29 x 10^{-4} cm [53]. Using the aforementioned τ_A value, and knowing the value of the A/V ratio, the permeability coefficient can be calculated. The permeability coefficient in this case is 13.2 x 10^{-4} cm/s. This value falls within the range of permeability coefficients for animal cell membranes that are presented by House [54].

It has been assumed in this study that for the various acute levels of edema, the permeability coefficient does not change. This assumption explains the use of a single value for τ_A as an input to the exchange model. If a more severe injury model were investigated, where tissue necrosis was present, the intracellular and extracellular mean water residence times in the context of exchange may have a greater effect on the values of the relaxation rates. In certain pathologies, such as muscular dystrophy, changes in the permeability of the cell membranes may create noticeable changes in exchange rates.

The use of quantitative relaxometric muscle imaging in the clinic is not as common as it is in small animal models, however there are some studies that have looked at changes in relaxation times with myopathy. A study by Maillard *et al*. investigated the changes in T_2 in the thigh muscles in children with juvenile dermatomyositis (JDM) [55]. It was found that the T_2 times in children with active JDM were significantly increased indicating an increase in muscle inflammation. Another study by Huang *et al*. used MR relaxometry to assess muscle status and monitor progression in patients with Duchenne Muscular Dystrophy (DMD) [56]. Huang found that dystrophic muscle presents with an increase in T_2 and a decrease in T_1 as fatty infiltration of the muscle occurs with necrosis. These studies, and others, suggest that these quantitative imaging techniques may be useful in not only recognizing but also monitoring treatment to various muscle pathologies.

The duration of the integrated measurements in this study prevent the clinical use of this particular protocol, though similar measurements might be made in less time by implementing accelerated protocols, such as a rapid acquisition transverse relaxometric (RATE) imaging sequence [57]. The clinical utility of this study is derived from the information of $\hat{T}_1$ changes with edema, though the actual relaxometric methods may have some clinical relevance as previously described. The observed change in $\hat{T}_{1B}$ with the apparent extracellular volume fraction may be useful in developing an inversion recovery protocol for selectively nulling tissue compartments based on the severity of muscle injury. These measurements could help form a relationship between the micro-anatomy and the changes in relaxation times with inflammation. It is possible that these techniques might help explain the exchange kinetics that occur with graded levels of muscle edema.

CHAPTER V

CONCLUSIONS

A graded edema model in rat hindlimb was produced by subcutaneous injections of λ-carrageenan at varying concentrations. Integrated T_1-T_2 measurements revealed two distinct signal components each with their own unique $\hat{T}_1$ and $\hat{T}_2$ times. It was found that the size of the long-lived compartment increased, with an increase in the concentration of λ-carrageenan, as did the $\hat{T}_1$ value of this signal component. Results from the simulation of the Bloch-McConnell equations in the context of a two-pool exchange model provided a comparison for the observed changes in the long-lived $\hat{T}_1$ component with a change in volume fraction. The data presented in this thesis further supports the notion that the two distinct compartments found with edema can be assigned to intracellular and extracellular water. In order to quantitatively relate these integrated measurements to the actual micro-anatomy, future studies will focus on obtaining independent measures of the extracellular volume fraction and more closely examining the exchange kinetics occurring with edema.

REFERENCES

[1] May DA, Disler DG, Jones EA, Balkissoon AA and Manaster BJ. Abnormal signal intensity in skeletal muscle at mr imaging: patterns, pearls, and pitfalls. *Radiographics* (2000) 20 Spec No: p. S295-315.

[2] Maillard SM, Jones R, Owens C, Pilkington C, Woo P, Wedderburn LR and Murray KJ. Quantitative assessment of MRI t2 relaxation time of thigh muscles in juvenile dermatomyositis. *Rheumatology (Oxford)* (2004) 43: pp. 603-608.

[3] Liu PT and Ilaslan H. Unicompartmental muscle edema: an early sign of deep venous thrombosis. *Skeletal Radiol.* (2003) 32: pp. 41-45.

[4] Hernandez RJ, Sullivan DB, Chenevert TL and Keim DR. Mr imaging in children with dermatomyositis: musculoskeletal findings and correlation with clinical and laboratory findings. *AJR Am J Roentgenol* (1993) 161: pp. 359-366.

[5] Shellock FG, Fukunaga T, Mink JH and Edgerton VR. Exertional muscle injury: evaluation of concentric versus eccentric actions with serial MR imaging. *Radiology* (1991) 179: pp. 659-664.

[6] Haacke EM, Brown RW, Thompson MR, and Venkatesan R. Magnetic Resonance Imaging: Physical Principles and Sequence Design. 1999.

[7] Hazlewood CF, Nichols BL and Chamberlain NF. Evidence for the existence of a minimum of two phases of ordered water in skeletal muscle. *Nature* (1969) 222: pp. 747-750.

[8] Hazlewood CF, Chang DC, Nichols BL, and Woessner DE. Nuclear magnetic resonance transverse relaxation times of water protons in skeletal muscle. *Biophys. J.* (1974) 14: pp. 583-606.

[9] Fung BM and Puon PS. Nuclear magnetic resonance transverse relaxation in muscle water. *Biophys. J.* (1981) 33: pp. 27-37.

[10] Civan MM, Achlama AM and Shporer M. The relationship between the transverse and longitudinal nuclear magnetic resonance relaxation rates of muscle water. *Biophys. J.* (1978) 21: pp. 127-136.

[11] Cole WC, LeBlanc AD and Jhingran SG. The origin of biexponential t2 relaxation in muscle water. *Magn Reson Med* (1993) 29: pp. 19-24.

[12] Gambarota G, Cairns BE, Berde CB and Mulkern RV. Osmotic effects on the t2 relaxation decay of in vivo muscle. *Magn Reson Med* (2001) 46: pp. 592-599.

[13] Ababneh Z, Beloeil H, Berde CB, Gambarota G, Maier SE and Mulkern RV. Biexponential parameterization of diffusion and t2 relaxation decay curves in a rat muscle edema model: decay curve components and water compartments. *Magn Reson Med* (2005) 54: pp. 524-531.

[14] Fan RH and Does MD. Compartmental relaxation and diffusion tensor imaging measurements in vivo in lambda-carrageenan-induced edema in rat skeletal muscle. *NMR Biomed* (2008) 21: pp. 566-573 .

[15] Nishimura DG. Principles of Magnetic Resonance Imaging. Ch.4. 1996.

[16] Block RE and Maxwell GP. Proton magnetic resonance studies of water in normal and tumor rat tissues. *J. Magn. Reson.* (1974) 14:pp. 329-334.

[17] English AE, Whittall KP, Joy MG, and Henkelman RM. Quantitative two-dimensional time correlation relaxometry. *Magn Reson Med* (1991) 22:pp. 425-434.

[18] de Certaines JD, Henriksen O, Spisni A, Cortsen M, and Ring PB. In vivo measurements of proton relaxation times in human brain, liver, and skeletal muscle: a multicenter MRI study. *Magn. Reson. Imag.* (1993) 11:pp. 841-850.

[19] Saab G, Thompson RT, Marsh GD, Picot PA, and Moran GR. Two-dimensional time correlation relaxometry of skeletal muscle in vivo at 3T. *Magn Reson Med* (2001) 46: pp. 1093-1098.

[20] Faure P, Doan BT, and Beloeil JC. In-vivo high resolution three-dimensional MRI studies of rat joints at 7T. *NMR Biomed* (2003) 16: pp. 484-493.

[21] Snaar JEM and Van As H. A method for simultaneous measurement of NMR spin-lattice and spin-spin relaxation times in compartmentalized systems. *J. Magn. Reson.* (1992) 99: pp. 139-148.

[22] Does MD and Gore JC. Compartmental Study of T1 and T2 in rat brain and trigeminal nerve in vivo. *Magn Reson Med* (2002) 47:pp. 274-283.

[23] Ploutz-Snyder LL, Nyren S, Cooper TG, Potchen EJ and Meyer RA. Different effects of exercise and edema on T2 relaxation in skeletal muscle. *Magn Reson Med* (1997) 37: pp. 676-682.

[24] Morvan D and Leroy-Willig A. Simultaneous measurements of diffusion and transverse relaxation in exercising skeletal muscle. *Magn Reson Imaging* (1995) 13: pp. 943-948.

[25] Morvan D. In vivo measurement of diffusion and pseudo-diffusion in skeletal muscle at rest and after exercise. *Magn Reson Imaging* (1995) 13: pp. 193-199.

[26] Lee RC, Despa F, Collins JC, Karczmar G and Tenchov B. Magnetic resonance imaging of muscle electroporation injury. *Conf Proc IEEE Eng Med Biol Soc* (2004) 7: pp. 5451-5454.

[27] Gissel H, Despa F, Collins J, Mustafi D, Rojahn K, Karczmar G and Lee R. Magnetic resonance imaging of changes in muscle tissues after membrane trauma. *Ann. N. Y. Acad. Sci.* (2005) 1066: pp. 272-285.

[28] Stekelenburg A, Oomens CWJ, Strijkers GJ, Nicolay K and Bader DL. Compression-induced deep tissue injury examined with magnetic resonance imaging and histology. *J. Appl. Physiol.* (2006) 100: pp. 1946-1954.

[29] Guay J, Bateman K, Gordon R, Mancini J and Riendeau D. Carrageenan-induced paw edema in rat elicits a predominant prostaglandin e2 (pge2) response in the central nervous system associated with the induction of microsomal pge2 synthase-1. *J. Biol. Chem.* (2004) 279: pp. 24866-24872.

[30] Lazzarini R, Paulino CA, Malucelli BE and Palermo-Neto J. Effects of high doses of diazepam on carrageenin-induced paw edema in rats. *Braz. J. Med. Biol. Res.* (1996) 29: pp. 1525-1529.

[31] Mense S. Nociception from skeletal muscle in relation to clinical muscle pain. *Pain* (1993) 54: pp. 241-289.

[32] Di Rosa M, Giroud JP and Willoughby DA. Studies on the mediators of the acute inflammatory response induced in rats in different sites by carrageenan and turpentine. *J. Pathol.* (1971) 104: pp. 15-29.

[33] McConnell HM. Reaction rates by nuclear magnetic resonance. *J Chem Phys* (1959) 28(3): pp. 430-431.

[34] Woessner DE. Brownian motion and its effects in NMR chemical exchange and relaxation in liquids. *Concepts in Magn Reson* (1996) 8(6): pp. 397-421.

[35] Woessner DE. Nuclear transfer effects in nuclear magnetic resonance pulse experiments. *J Chem Phys* (1961) 35: pp. 41-48.

[36] Majumdar S, Orphanoudakis SC, Gmitro A, O'Donnell M, and Gore JC. Errors in the measurements of T2 using multiple-echo MRI techniques: I. Effects of radiofrequency pulse imperfections. *Magn Reson Med* (1986) 3: pp. 397-417.

[37] Majumdar S, Orphanoudakis SC, Gmitro A, O'Donnell M, and Gore JC. Errors in the measurements of T2 using multiple-echo MRI techniques: I. Effects of static field inhomogeneity. *Magn Reson Med* (1986) 3: pp. 562-574.

[38] Skinner MG, Kolind SH, and MacKay AL. The effect of varying echo spacing within a multiecho acquisition: better characterization of long T2 components. *Magn Reson Imag* (2007) 25: pp. 840-847.

[39] Levitt MH and Freeman R. Compensation for pulse imperfections in NMR spin-echo experiments. *J Magn Reson* (1981) 43: pp. 65-80.

[40] Crawley AP and Henkelman RN. Errors in T2 estimation using multi-slice multiple-echo imaging. *Magn Reson Med* (1987) 4: pp. 33-47.

[41] Zur Y. and Stokar S. A phase-cycling technique for canceling spurious echoes in NMR imaging. *J Magn Reson* (1987) 71: pp. 212-228.

[42] Cieslar J, Huang M, and Dobson G. Tissue spaces in rat heart, liver, and skeletal muscle in vivo. *Am J Physiol Regulatory Integrative Comp Physiol* (1998) 275: pp. 1530 – 1536.

[45] Donahue KM, Weisskoff RM, Parmelee DJ, Callahan RJ, Wilkinson RA, Mandeville JB, and Rosen BR. Dynamic Gd-DTPA enhanced MRI measurements of tissue cell volume fraction. *Magn Reson Med* (1995) 34: pp. 423-432.

[44] Landis CS, Li X, Telang FW, Molina PE, Palyka I, Vetek G, and Springer Jr. CS. Equilibrium transcytolemmal water-exchange kinetics in skeletal muscle in vivo. *Magn Reson Med* (1999) 42: pp. 467-478.

[45] Bilgen M, Al-Hafez B, Malone T, and Smirnova I. Ex vivo magnetic resonance imaging of rat spinal cord at 9.4T. *Magn Reson Imag* (2005) 23: pp. 601-605.

[46] Bonny JM, Zanca M, Boire JY, R, and Veyre A. T_2 maximum likelihood estimation from multiple spin-echo magnitude images. *Magn Reson Med* (1996) 36: pp. 287-293.

[47] Whittall KP and MacKay AL. Quantitative interpretation of NMR relaxation data. *J Magn Reson* (1989) 84: pp. 134-152.

[48] Lawson CL and Hanson RJ. Solving least squares problems. Englewood Cliffs, NJ. Prentice-Hall; (1974).

[49] Chen JH, Avram HE, Crooks LE, Arakawa M, Kaufman L, and Brito AC. In vivo relaxation times and hydrogen density at 0.063-4.85T in rats with implanted mammary andenocarcinomas. *Radiology* (1992) 184: pp. 427-434.

[50] Gold GE, Han E, Stainsby J, Wright G, Brittain J, and Beaulieu C. Musculoskeletal MRI at 3.0T: Relaxation times and image contrast. *Am J Roentg* (2004) 183: pp. 343-351.

[51] Duewell SH, Ceckler TL, Ong K, Wen H, Jaffer F, Chesnick S, and Balaban R. Musculoskeletal MR imaging at 4.0T and at 1.5T: Comparison of relaxation times and image contrast. *Radiology* (1995) 196: pp.551-555.

[52] Radhakrishnan R, Moore SA, and Sluka K. Unilateral carrageenan injection into muscle or joint induces chronic bilateral hyperalgesia in rats. *Pain* (2003) 104: pp.567-577.

[53] Ustunel I and Demir R. A histochemical, morphometric, and ultrastructural study of gastronemius and soleus muscle fiber type composition in male and female rats. *Acta Anatomica* (1997) 158: pp.279-286.

[54] House CR. Water transport in cells and tissues. *London UK: Edward Arnold Ltd.* (1974) pp. 152-161.

[55] Maillard SM, Jones R, Owens C, Pilkington C, Woo P, Wedderburn LR, and Murray KJ. Quantitative assessment of MRI T_2 relaxation time of thigh muscle in juvenile dermatomyositis. *Rheumatology* (2004) 43: pp. 603-608.

[56] Huang Y, Majumdar S, Genant H, Chan W, Sharma K, Yu P, Mynhier M, and Miller R. Quantitative MR relaxometry study of muscle composition and function in Duchenne Muscular Dystrophy. *J. Magn Reson Imag* (1994) 4: pp. 59-64.

[57] Does MD and Gore JC. Rapid Acquisition Transverse Relaxometric Imaging. *J. Magn Reson* (2000) 147: pp. 116-120.